Institut für Plasmaphysik

KERNFORSCHUNGSANLAGE JÜLICH

des Landes Nordrhein-Westfalen

Density Distributions from Radiation
Measurents During the Fast Magnetic
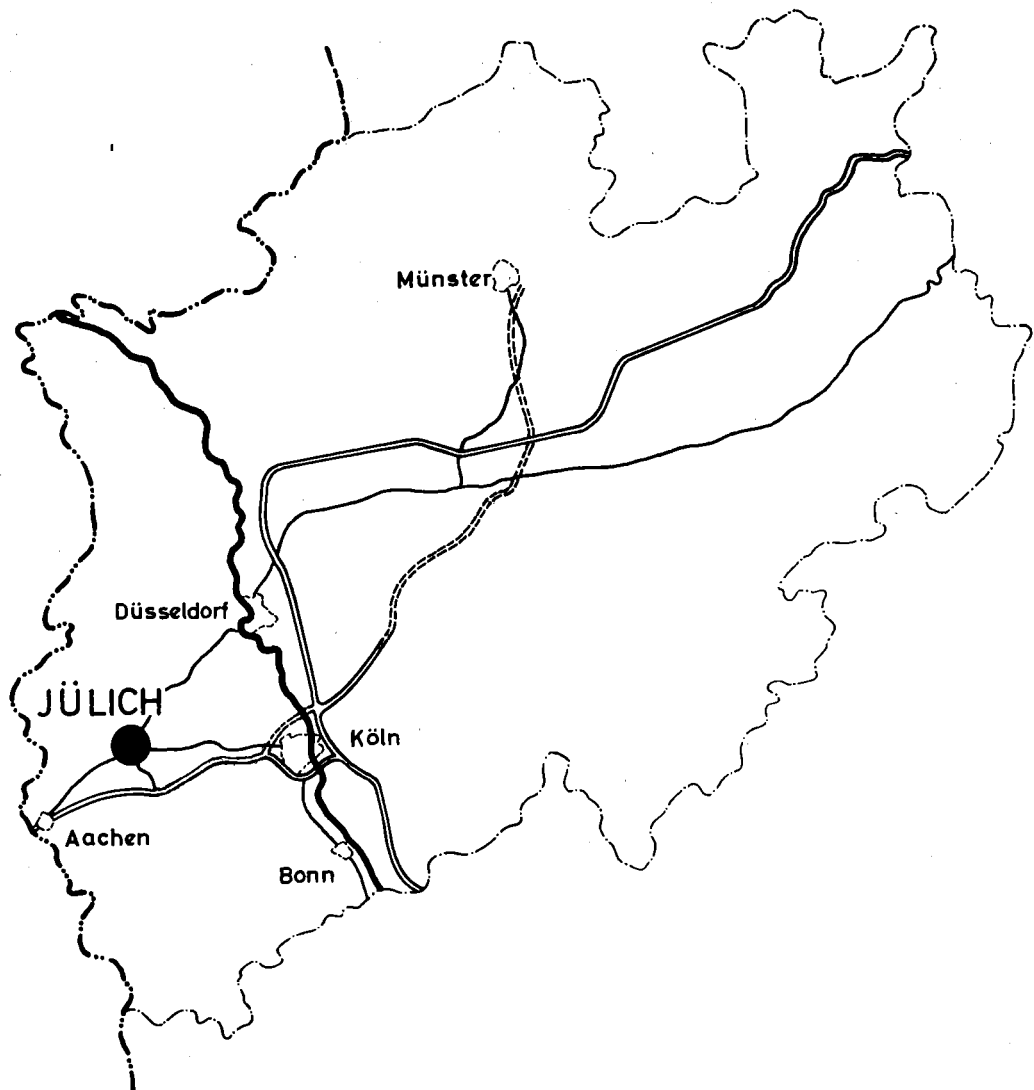# Compression of a Plasma

by

P. Bogen and E. Hintz

Berichte der Kernforschungsanlage Jülich — Nr. 18

Institut für Plasmaphysik Jül — 18 — PP

Density Distributions from Radiation Measurents During the Fast Magnetic Compression of a Plasma.

by

P. Bogen and E. Hintz[*]

Institut für Plasmaphysik, Kernforschungsanlage Jülich/Germany

I. Introduction

For the fast magnetic compression of a deuterium plasma, as described in another paper of this conference, (1), the compression ratio and end losses are of high interest. For the determination of these quantities the radial density distribution must be known as a function of time.

Present theoretical calculations, concerned with the fast compression of plasma with parallel or reverse magnetic bias field are in need of experimental data, which also can be taken from density and intensity distributions.

This information can partly be obtained from smear camera pic-

[*]Paper presented at the Conference on Plasma Physics and Controlled Nuclear Fusion Research, Salzburg 1961.

tures. For this purpose the film density must be transformed
into light intensity. The interpretation of the intensity dis-
tribution requires information on the composition of plasma ra-
diation and on the dependence of the intensity on plasma densi-
ty and temperature. In some cases the density distributions can
be derived from the observed intensity.

II. Determination of densities from intensity measurements.

The observed radiation may be composed of

1. Impurity radiation

2. Line radiation

3. Free-bound radiation

4. Free-free radiation

The contribution of the impurity radiation to the observed
light intensity was determined experimentally, because a theore-
tical calculation was believed to be impossible. For this pur-
pose pure hydrogen was mixed with methane or oxygen.

From the increase of the intensity of C or O spectral lines as
functions of the added amount of impurity the concentration of
C and O in the "pure" hydrogen plasma can be determined. The

contribution of impurities to the total visible radiation was
estimated in a similar way.

The line radiation intensity is given by

$$I = \frac{1}{4\pi} \quad A_{n\,m} \quad h \cdot \nu \; N_i N_e \frac{h^3}{(2\pi mkT)^{3/2}} \quad n^2 \quad \exp(U_n/KT),$$

$A_{n\,m}$ = transition probability, N_i = ion density,

T   = electron temperature, N_e = electron density,

n   = quantum number of the upper level,

U_n = ionization energy from the upper level,

the free-bound radiation intensity by

$$I = C \cdot \int g_{fb} \frac{2\,U_1}{(K\,T)^{3/2}} \quad N_i \, N_e \left[\sum_n \frac{1}{n^3} \exp\,(U_n/KT) \right] \exp(-h\nu/KT)\,d\nu$$

g_{fb} = free bound Gaunt factor, C = 6,36 $\cdot$ 10^{-47} cgs units.
The free-free radiation intensity by

$$I = C \cdot \int g_{ff} \frac{N_i \, N_e}{(K\,T)^{1/2}} \quad \exp \quad (-h\nu/KT) \; d\nu$$

These equations show that the intensities of different kinds of
hydrogen radiation are proportional to $N_i \, N_e$, but they depend
on the temperature in a different way. In all cases the exponen-
tial is close to one if T is higher than 10 eV. Furthermore, at
these temperatures the intensity of free-free radiation is

higher than that of the free-bound and line radiations together.
Therefore, with $T_e > 10$ eV and $N_i = N_e$ one gets

$$N_i \sim I^{1/2} \cdot (kT)^{1/4}$$

As N_i is only weakly dependent on T the assumption that the temperature across the diameter of the plasma is nearly constant, can often be used for the quantitative interpretation of smear camera pictures.

As will be shown later, this assumption is not correct in all cases. At low temperatures (1-10 eV) a simple test can be made by photographing the discharge one time in the light between 3 700 A - 6 400 A and another time in the light between 5 100 A and 6 400 A. Caused by hydrogen line radiation, the region between 3 700 and 5 100 A is very sensitive to temperature changes. If no strong temperature gradient exists, the pictures must be identical in both spectral regions.

III. Methods of measurement.

The smear camera pictures were taken from the discharge with a Beckmann 339b streak camera. A slit width of 0,15 mm was chosen, giving a time resolution of $2 \cdot 10^{-8}$ sec at 2 600 r.p.s.

Observations have been made both side on and end on. Intensity distributions taken from side on pictures can be transformed into radial distributions in the case of rotational symmetry by Abel's integral equation. As this symmetry is not always completely given, the interpretation of results has to be done with care.

End on pictures give directly the intensity distribution I (r). But this intensity is integrated over inhomogeneous zones parallel to the axis of the plasma cylinder. The plasma region not focused gives a broadening of the observed diameter.

Because both side on and end on observations have their advantages and disadvantages, in one case the plasma was photographed by both methods under identical conditions. Unfortunately, at lower densities side on observations were impossible because the intensity was not high enough.

The standardization of the films was performed by a Pt-filter at the slit of a quartz spectrograph. As light source, a spark with a duration of about 0.2 μsec was used. This way, the error caused by the Schwarzschild exponent was made as low as possible. The standardization could be obtained for all wavelengths

between 3 700 and 6 400 A. But the error in the intensity dis-
tribution caused by neglecting wavelength dependence was lower
than 10%, if the standardization at 5000 A was taken.

The intensity distributions obtained from the densitometer cur-
ves were plotted in a logarithmic scale. If the numbers on the
scale are devided by two, the density distributions are obtained.

At low film densities errors must be expected from stray-light,
caused by the camera, by low temperature plasma in front of the
high temperature zone, and by light from the hot quartz tube.
This effects that the measured intensity differences are lower
than in reality.

IV. Results.

The observed impurity radiation belongs to oxygen and carbon.
Fig.1 shows the intensity of a C V spectral line as a function
of the added amount of methane. Extrapolating the plot to zero
intensity a concentration of 0.02% carbon in the "pure" hydro-
gen is estimated. From the second curve of this figure a con-
tribution of carbon to the visible radiation below 10% was con-
cluded.

In the same way the percentage of oxygen in the "pure" hydrogen was estimated to be lower than 0.04%. Fig.2 shows the intensity of an O V line in a discharge in "pure" hydrogen and in 230 μ (H_2 + $\frac{1}{760}$ O_2). In the second half cycle both amplitudes are equal, whereas in the first half-cycle the amplitude in pure gas is much lower than with oxygen added. It follows, that the impurities come mainly from the walls at the end of the first half-cycle caused by interaction of plasma with the walls and not by high electric fields at the start of the first half-cycle.

As was shown, the plasma is of high purity in the first half-cycle, and it is possible to neglect the impurity radiation in the visible region. Therefore the observed radiation can belong only to hydrogen and is proportional N_i N_e.

In figs.3,4 end on and side on intensity distributions of the discharge without a magnetic bias field at a line density of 2.2 · 10^{17}/cm are given.

The observed side on intensity distribution was transformed by Abel's integral equation. From this figure the following conclusions can be drawn:

1. The intensity distributions obtained end on and side on
   are not exactly equal. The halfwidth observed side on has a
   maximum deviation of 30% from the "end on" measurement. The
   plasma diameter can be defined by the halfwidth of the den-
   sity distribution. Then one obtains from side on observation
   a volume compression of 1:20 at the first maximum compres-
   sion and of 1:26 at the second maximum compression. From
   end on observation, lower ratios are calculated.

2. At the first compression the intensity has its maximum in
   the centre of the tube. But in the following expansion, the
   intensity in the centre amounts to 60% of the maximum inten-
   sity. Consequently the ratio of the maximum density to the
   density on the tube axis is 1:0.75.

3. The intensity side on decreases faster than the intensity
   end on which may be caused by density variations along the
   axis.

4. An upper limit for the end losses can be obtained by compa-
   ring the line densities at the second compression maximum
   and 0.8 μsec later. The integration across the radius must
   be interrupted at a certain value to reduce the contribution
   from stray light. The integration is terminated both times
   at the same value of r, to obtain the volume mass losses.
   Assuming that the temperature is only increasing, we obtain
   a mass loss lower than 30%.

As mentioned before, at lower pressures only end on photographs
were possible. In fig.5 the smear camera pictures of the dis-
charge without a magnetic bias field at a line density of

$1.1 \cdot 10^{17}$/cm and with parallel or antiparallel magnetic bias field at a line density of $8.8 \cdot 10^{16}$/cm are given. From these photographs the intensity distributions were evaluated (fig.6-8).

The dynamic behaviour of the plasma without a magnetic bias field at a line density of $1.1 \cdot 10^{17}$/cm is similar to that at higher density. The average plasma diameter between compression and expansion decreases with increasing field as expected. But at the low line densities used in fig.6, even with decreasing field the diameter decreases. This phenomenon can be explained by assuming that the kinetic pressure decreases faster than the magnetic pressure (1).

The interpretation of intensity distributions of plasma with strong internal magnetic field is difficult, because temperature inhomogeneities must be expected caused by the low thermal conductivity across the magnetic field.

With a steady magnetic field parallel to the external field the intensity distribution has two maxima at the first compression. But the picture in the light between 5 100 and 6 400 A shows only one maximum. As mentioned before, the second maximum therefore is due to the low plasma temperature in that region. The intensity minimum in the axis can not be understood by a density effect, because the magnetic field measurements give a homogeneous distribution. But as shown by theoretical calculations (3) a strong increase of the electron temperature is to be expected in the centre causing a minimum in the intensity

distribution.

In the following oscillations, this intensity distribution is frozen in. This is to be expected due to the low field diffusion. Probably the temperature distribution will likewise be unchanged due to low thermal conductivity.

In the case of antiparallel magnetic bias fields, there is a high magnetic field gradient caused by high currents in the sheath between parallel and antiparallel fields. Because a part of the antiparallel field is dissipated in this layer, a mass flow results from the central part to the plasma boundary. As a consequence there should be a hole in the density distribution at the centre. In this case the temperature differences between the centre and the intensity maximum seem to be not very high (3). The observed minimum of the intensity in the centre can then only be understood by a density minimum.

As can be seen from the following plots, the sheath broadens rapidly, and the hole disappears after about three oscillations. At higher densities it can be observed during the whole discharge.

V. Summary

Since the plasma observed has a low impurity concentration, only the hydrogen radiation has to be taken into account for the interpretation of smear camera pictures. This radiation is proportional to N_i^2. Without a steady magnetic field, it seems pos-

sible to neglect the radial temperature inhomogeneity for the calculation of the density distribution.

Side on and end on photographs give not exactly the same results for the radius of the plasma and for the intensity as function of time. The differences are probably caused by inhomogeneities of the density along the axis. Side on observations have the disadvantage that for the calculation of the radial intensity distribution radial symmetry is necessary. In the case discussed above this seems to be allowed because no eruptions etc. were observed.

In this way it could be shown in one case that particle losses are lower than 30%. At lower pressures end losses seem to be higher. The plasma radius decreases even after the magnetic field has reached its maximum. This can be understood by mass losses because a rapid temperature decrease is not expected by theory. Furthermore, in this case an increase of the intensity should be observed which is not the case.

For an accurate calculation of densities from intensities in the case of strong trapped magnetic fields, a measurement of the radial temperature distribution is necessary. Without this only a rough estimate for a plasma with trapped antiparallel field is possible. A comparison with theoretical calculations (3) shows that the intensity minimum observed on the axis cannot be attributed to temperature differences alone. A density minimum must be therefore in the centre.

References:

1. Hintz, E., Conference on Plasma Physics and Controlled
   Nuclear Fusion Research, Salzburg, 1961.
2. Hain, K., private communication.
3. Hain, K., private communication.

Captions:
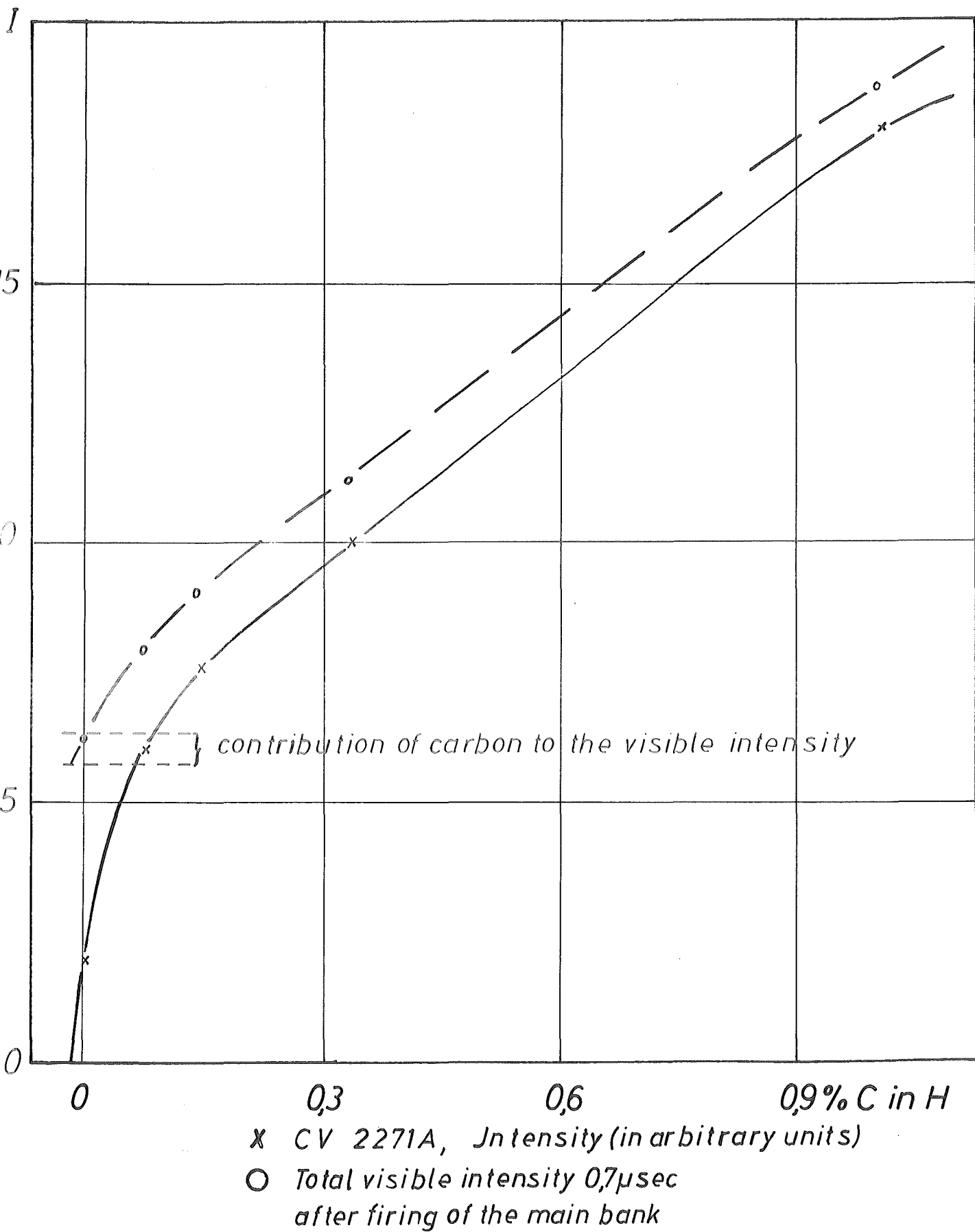
Fig.1 Intensity of a CV spectral line and of the total visible
       radiation as a function of the added amount of C at a
       pressure of 230μ H_2.

Fig.2 Total visible radiation and OV spectral line at a pres-
       sure of 230μ H_2 (a) and 230μ $(H_2 + 1/760 \ O_2)$ (b).

Fig.3 Radial intensity distributions observed end on in D_2
       Line density $N = 2.2 \cdot 10^{17} cm^{-1}$.

Fig.4 Radial intensity distribution observed side on in D_2
       after transformation with Abel's integral equation. Line
       density $N = 2.2 \cdot 10^{17} cm^{-1}$.

Fig.5 Smear camera pictures without and with a steady magnetic
       field of 2 500 Gauss.

Fig.6 Radial intensity distributions observed end on in D_2.
       Line density $1.1 \cdot 10^{17} cm^{-1}$.

Fig.7 Radial intensity distributions observed end on in D_2.
       Line density $8.8 \cdot 10^{16} cm^{-1}$. $B_{z_0} = + 2$ 500 Gauss.

Fig.8 Radial intensity distribution observed end on in D_2.
       Line density $8.8 \cdot 10^{16} cm^{-1}$. $B_{z_0} = -2$ 500 Gauss.

Fig.1 Jntensity of a CV spectral line and of the total visible intensity as a function of the added amount of C at a pressure of 230μ H
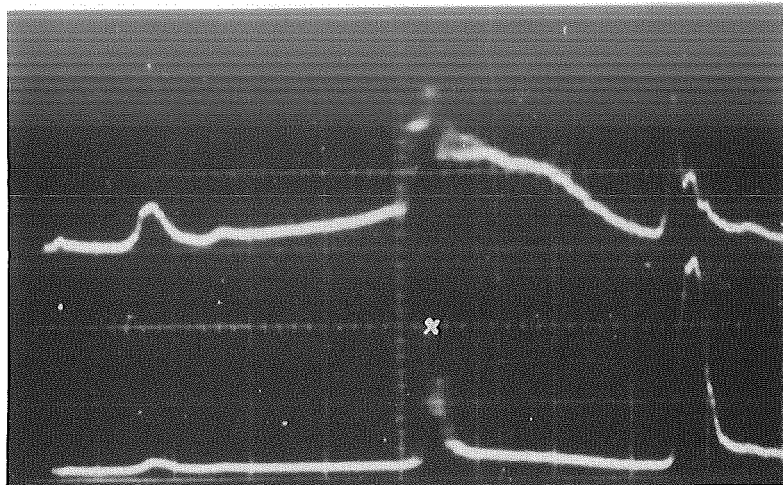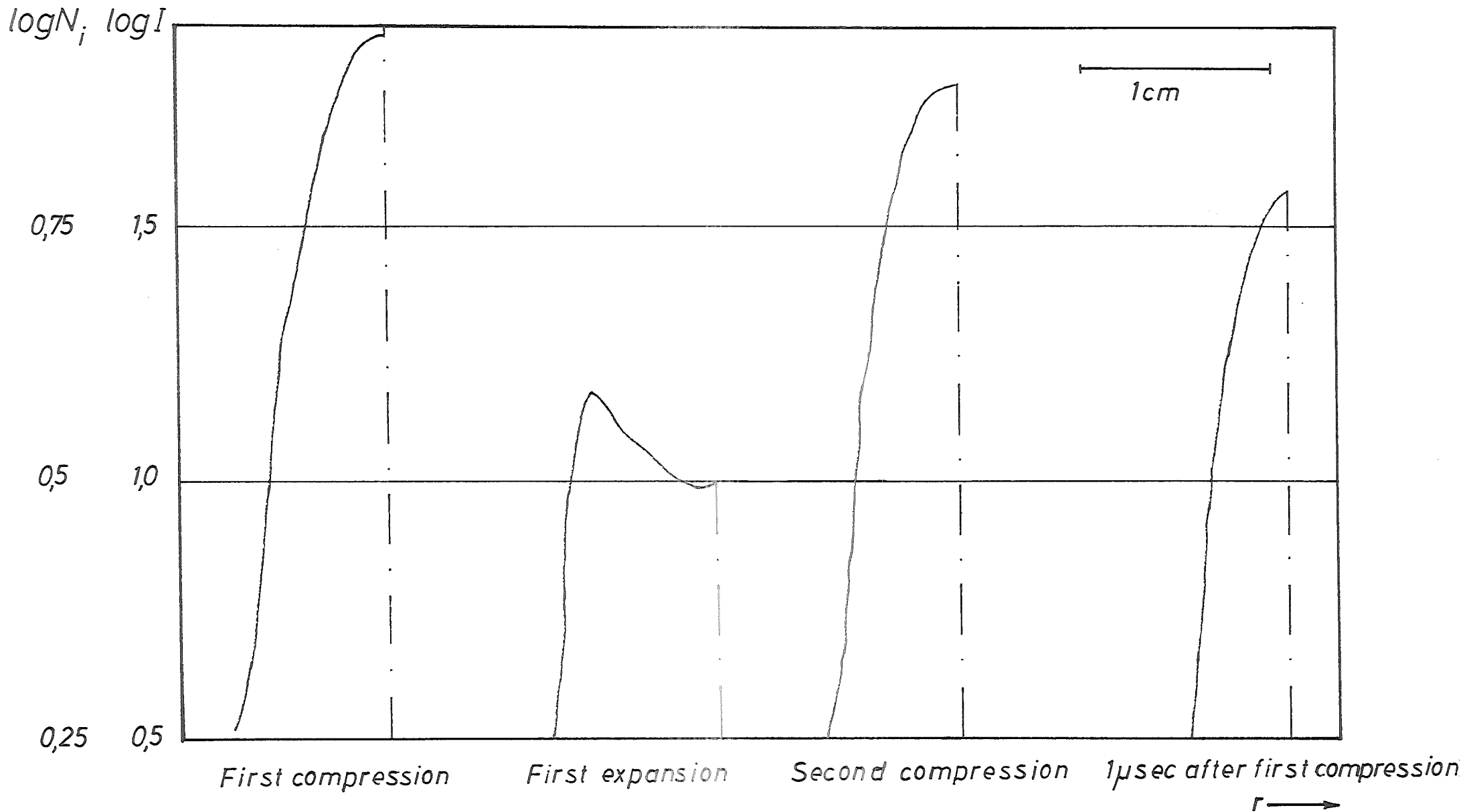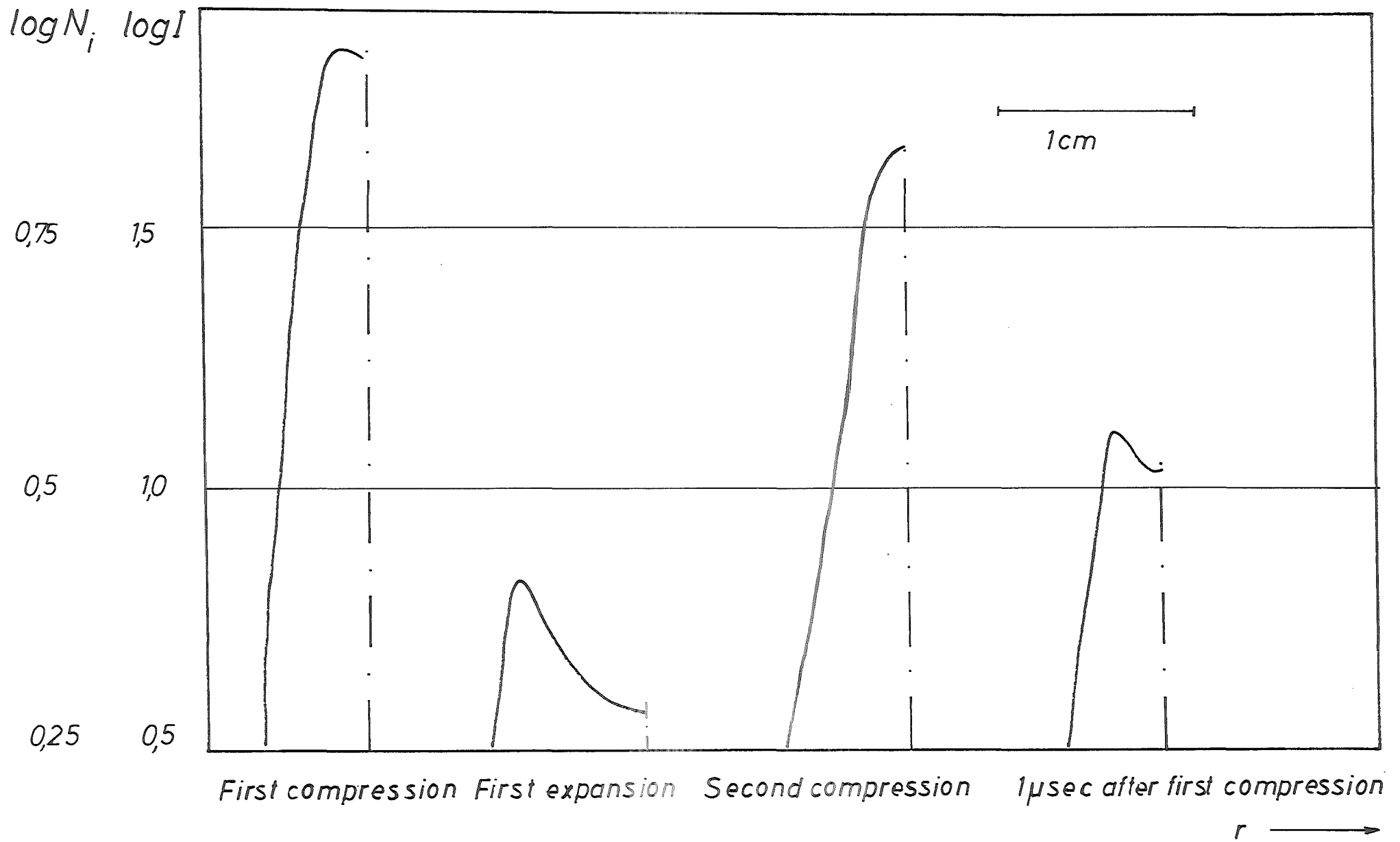
a)
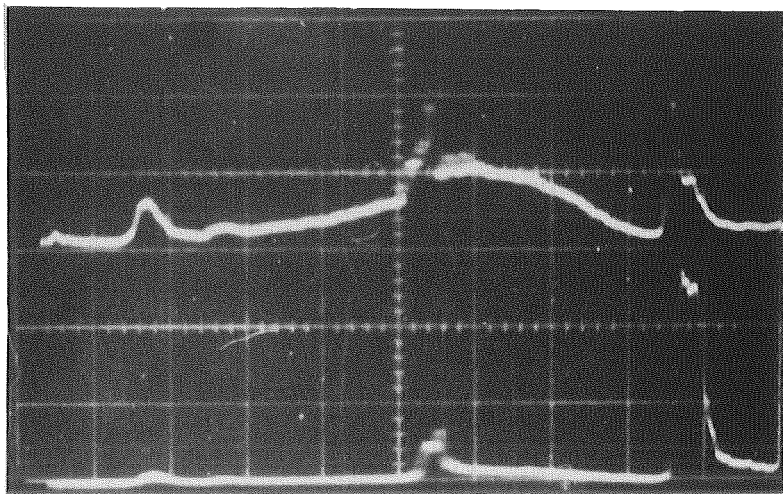
Total visible
radiation

O$\underline{\text{V}}$ 2478 Å

b)

Total visible
radiation

O$\underline{\text{V}}$ 2478 Å

Time scale 0,5 μsec/div.
(x Maximum intensity)

Fig. 2 Total visible radiation and OV spectral line at
a pressure of 230μ H$_2$ (a) and 230μ H$_2$ +1/760 O$_2$ (b).

Fig.3 Radial intensity distributions observed end on in D_2. Line density $N = 2.2 \cdot 10^{17} cm^{-1}$

Fig. 4 Radial intensity distribution observed side on in D_2 after transformation with Abel's integral equation. Line density $N = 2.2 \cdot 10^{17}\,cm^{-1}$.

$$B_{z_0} = 0 \; Gauss$$

1 μsec

$$B_{z_0} = {}^+2500 \; Gauss$$

1 μsec
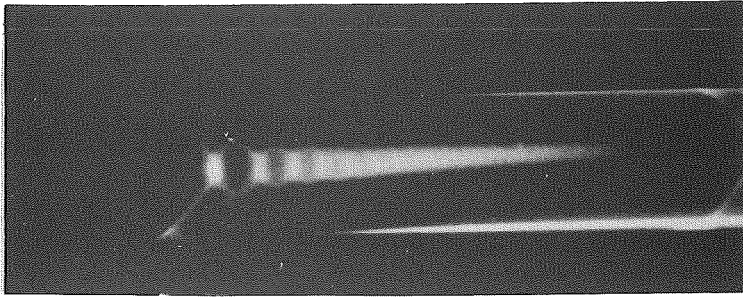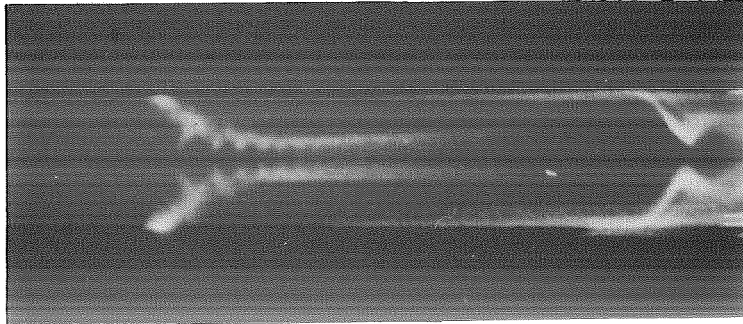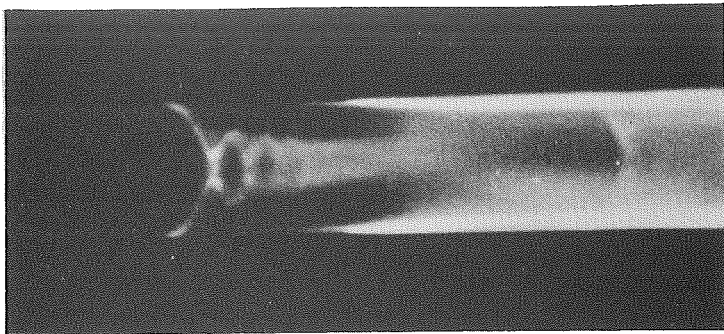
$$B_{z_0} = -2500 \; Gauss$$

1 μsec

Fig. 5 Smear camera pictures without and
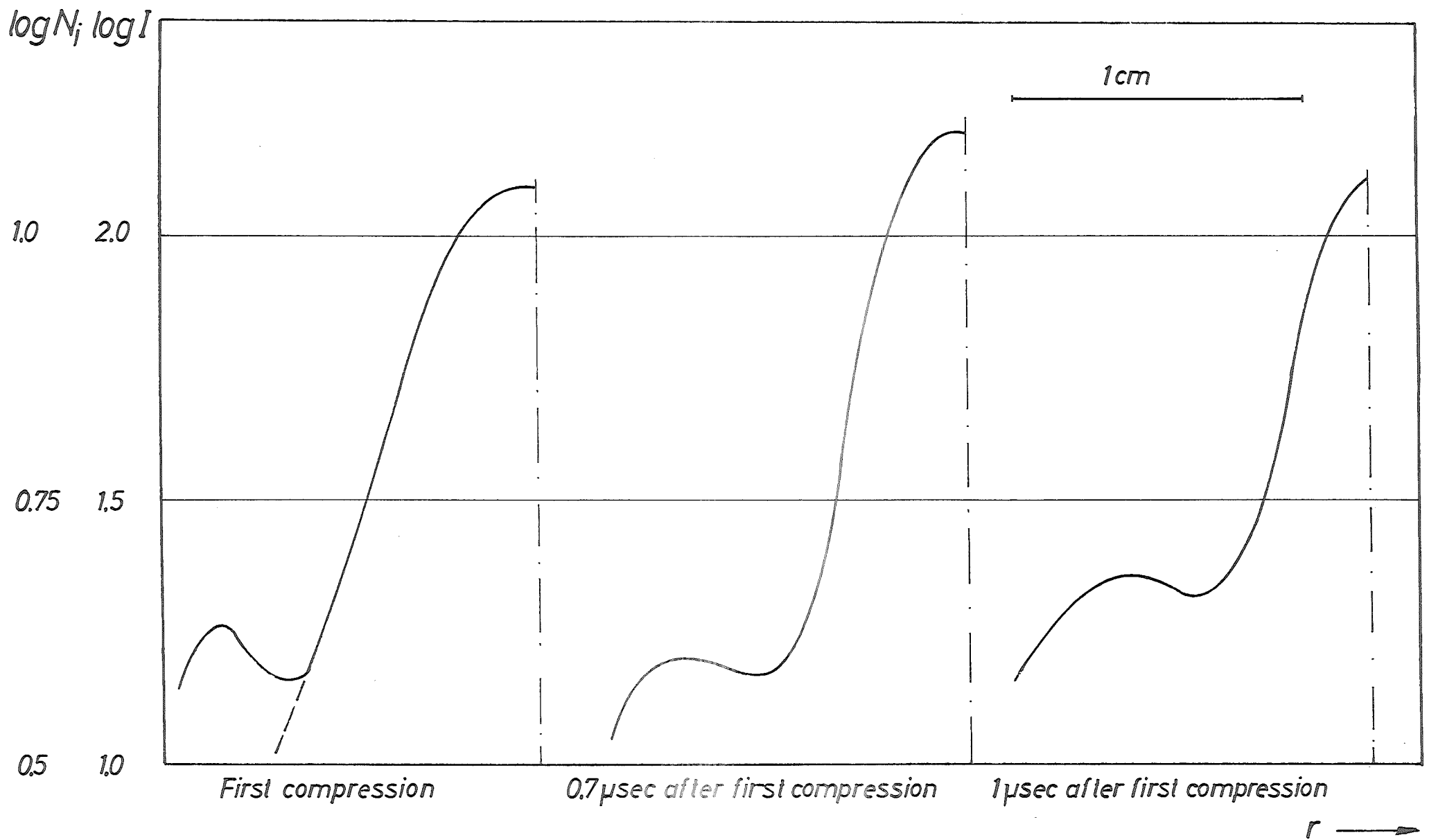with a steady magnetic field of 2500 Gauss.

Fig.6 Radial intensity distributions observed end on in D_2. Line density $1.1 \cdot 10^{17} cm^{-1}$.
_ _ _ intensity distribution with filler.
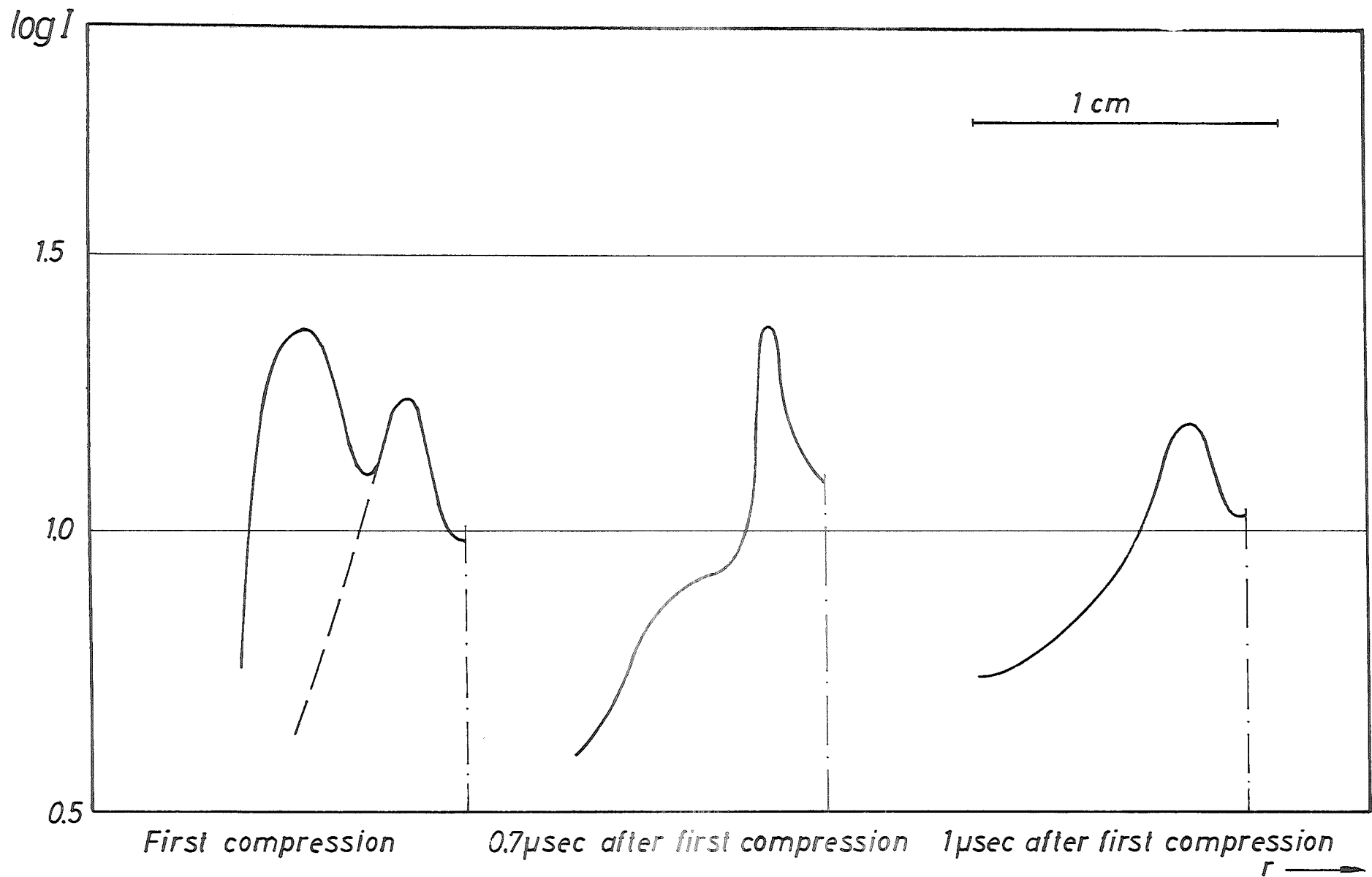
Fig.7 Radial intensity distribution observed end on in D_2. Line density $8.8 \cdot 10^{16} cm^{-1}$. $B_{z_0} = +2500$ gauss.
___ intensity distribution with filter.

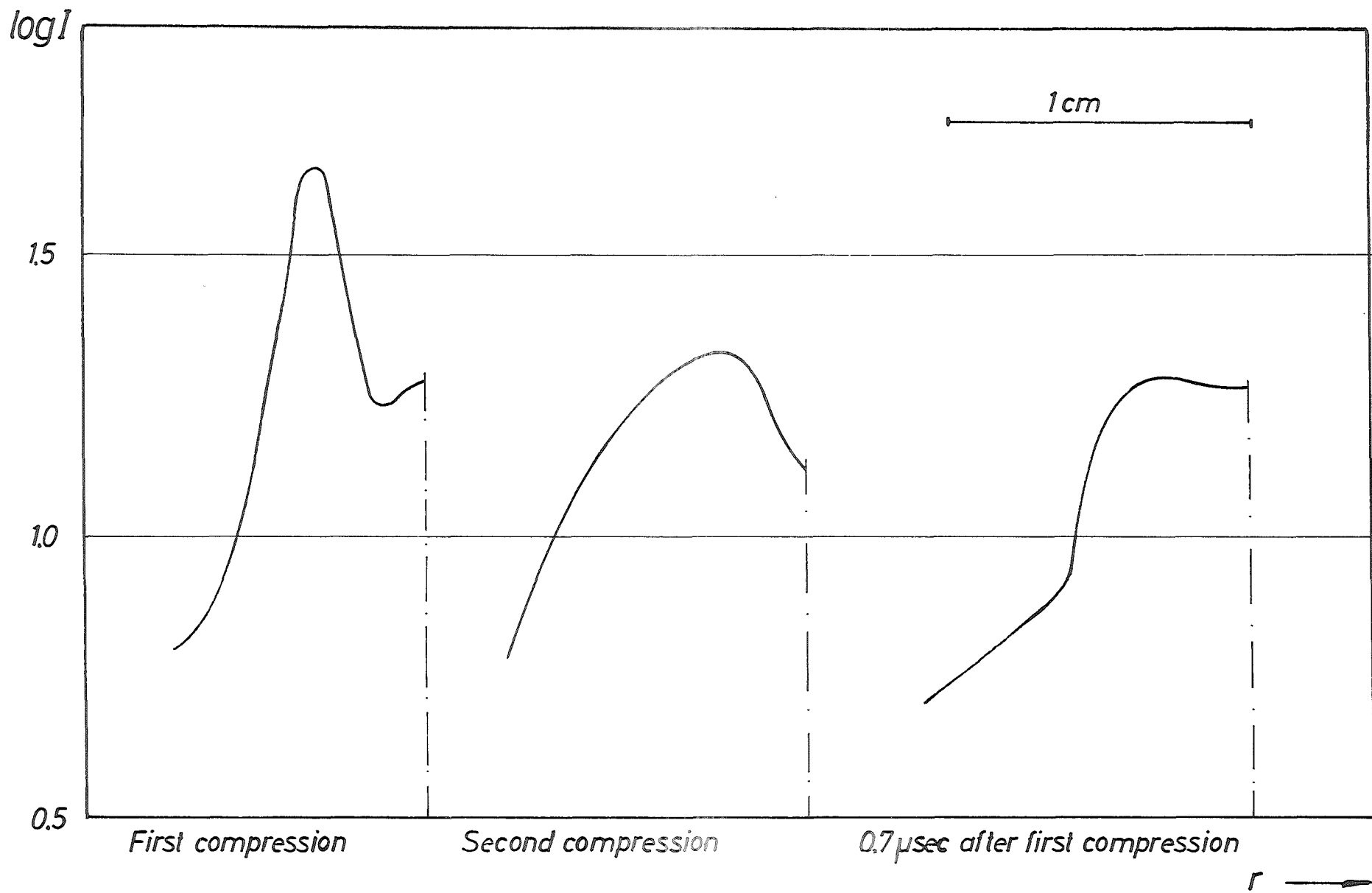Fig. 8 Radial intensity distribution observed end on in D_2. Line density $8.8 \cdot 10^{16} cm^{-1}$. $B_{z_0} = -2500$ gauss.